

CM² MAGAZINE



第 126 期



南方科技大学海洋磁学中心主编

<http://cm2.sustech.edu.cn/>

创刊词

海洋是生命的摇篮，是文明的纽带。地球上最早的生命诞生于海洋，海洋里的生命最终进化成了人类，人类的文化融合又通过海洋得以实现。人因海而兴。

人类对海洋的探索从未停止。从远古时代美丽的神话传说，到麦哲伦的全球航行，再到现代对大洋的科学钻探计划，海洋逐渐从人类敬畏崇拜幻想的精神寄托演变成可以开发利用与科学研究的客观存在。其中，上个世纪与太空探索同步发展的大洋科学钻探计划将人类对海洋的认知推向了崭新的纬度：深海（deep sea）与深时（deep time）。大洋钻探计划让人类知道，奔流不息的大海之下，埋藏的却是亿万年的地球历史。它们记录了地球板块的运动，从而使板块构造学说得到证实；它们记录了地球环境的演变，从而让古海洋学方兴未艾。

在探索海洋的悠久历史中，从大航海时代的导航，到大洋钻探计划中不可或缺的磁性地层学，磁学发挥了不可替代的作用。这不是偶然，因为从微观到宏观，磁性是最基本的物理属性之一，可以说，万物皆有磁性。基于课题组的学科背景和对海洋的理解，我们对海洋的探索以磁学为主要手段，海洋磁学中心因此而生。

海洋磁学中心，简称 CM^2 ，一为其全名“Centre for Marine Magnetism”的缩写，另者恰与爱因斯坦著名的质能方程 $E = MC^2$ 对称，借以表达我们对科学巨匠的敬仰和对科学的不懈追求。

然而科学从来不是单打独斗的产物。我们以磁学为研究海洋的主攻利器，但绝不仅限于磁学。凡与磁学相关的领域均是我们关注的重点。为了跟踪反映国内外地球科学特别是与磁学有关的地球科学领域的最新研究进展，海洋磁学中心特地主办 CM^2 Magazine，以期与各位地球科学工作者相互交流学习、合作共进！

“海洋孕育了生命，联通了世界，促进了发展”。21 世纪是海洋科学的时代，由陆向海，让我们携手迈进中国海洋科学的黄金时代。

目录

1. 次表层水超前于海因里希事件.....	1
2. 埃特纳火山灰岩石磁学特征.....	4
3. 碰撞引发的俯冲起始:基于实例和模型的综述.....	8
4. 过去 2000 年东亚-太平洋模式和 ENSO 对长江流域中部百年尺度水文气候变化的调制	10
5. 青藏高原东南部全新世中-晚期相对温暖的证据.....	13
6. 中世纪气候异常期间的古环境条件、小冰期和中美洲东部地区的社会影响.....	15
7. 来自以色列北部更新世古强度结果:时间平均地磁场半球不对称性的意义.....	18
8. 晚中新世冷却与二氧化碳耦合具有类似更新世的气候敏感性.....	20
9. 南大西洋福克兰群岛晚冰期—全新世南半球西风变化记录.....	23
10. 格陵兰冰芯记录中格陵兰变暖时间的综合不确定性估计.....	26

1. 次表层水超前于海因里希事件

翻译人: 仲义 zhongy@sustech.edu.cn



Max L, Nürnberg D, Chiessi C M, R G, et al. *Subsurface ocean warming preceded Heinrich Events* [J] *Nature Communications*, 2022, 13(1), 4217.

<https://doi.org/10.1038/s41467-022-31754-x>

摘要: 虽然在海因里希事件期间劳伦冰盖不稳定对冰川气候具有重要的影响,但是驱动这些冰原不稳定的机制仍不清楚。本文报道了在北大西洋地区西部亚极地采集的沉积物岩心中,基于有孔虫的次表层(水深~150 m)海洋温度和盐度的重建,显示在过去 27000 年同一岩心中发现海因里希事件转变之前,海洋次表层快速变暖的一致模式。这些结果首次提供了重要的证据,证实海洋热量在临界深度附近大量积累,触发了拉布拉多海附近的劳伦冰盖海洋末端部分的融化。大西洋亚极地地区次表层热源的反复积累与大西洋径向翻转流减弱的时间密切相关,表明海因里希事件期间海洋环流变化对引发冰盖突变不稳定具有前兆作用。作者推断未来较弱的海洋环流可能导致亚极地大西洋内部变暖加速,这可能会对现代北极海洋冰川和北大洋淡水收支的稳定至关重要。

ABSTRACT: Although the global environmental impact of Laurentide Ice-Sheet destabilizations on glacial climate during Heinrich Events is well-documented, the mechanism driving these ice-sheet instabilities remains elusive. Here we report foraminifera-based subsurface (~150 m water depth) ocean temperature and salinity reconstructions from a sediment core collected in the western subpolar North Atlantic, showing a consistent pattern of rapid subsurface ocean warming preceding the transition into each Heinrich Event identified in the same core of the last 27,000 years. These results provide the first solid evidence for the massive accumulation of ocean heat near the critical depth to trigger melting of marine-terminating portions of the Laurentide Ice Sheet around Labrador Sea followed by Heinrich Events. The repeated build-up of a subsurface heat reservoir in the subpolar Atlantic closely corresponds to times of weakened Atlantic Meridional Overturning Circulation, indicating a precursor role of ocean circulation changes for initiating abrupt ice-sheet instabilities during Heinrich Events. We infer that a weaker ocean circulation in future may result

in accelerated interior-ocean warming of the subpolar Atlantic, which could be critical for the stability of modern, marinerterminating Arctic glaciers and the freshwater budget of the North Atlantic.

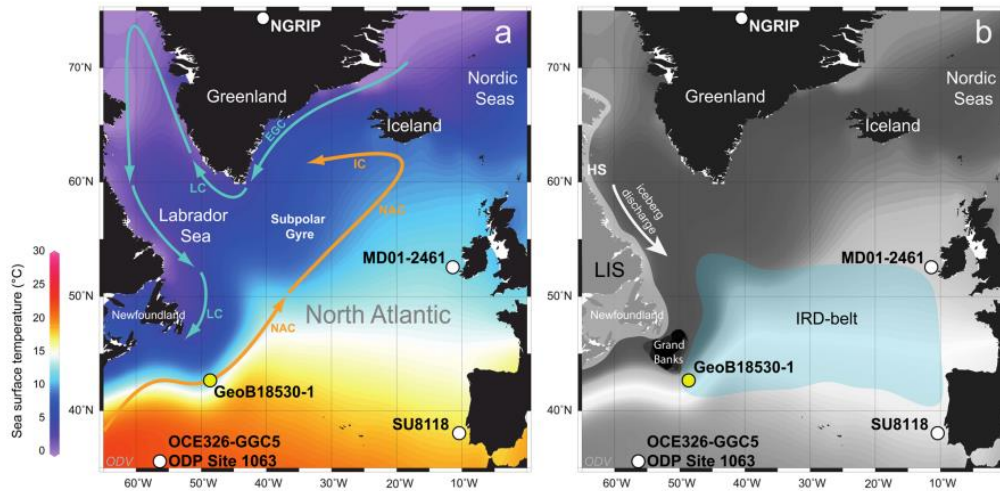


Figure 1. Modern surface-ocean conditions in the North Atlantic, the extension of the Laurentide Ice Sheet (LIS) and the IRD-belt in the North Atlantic during the Last Glacial Maximum. (a) Annual mean sea surface temperature (colour shading) and surface circulation (arrows) in the study area. Yellow dot: location of core site GeoB18530-1 (42° 50' N, 49° 14' W; 1,888 m water depth; this study); white dots: location of reference core sites MD01-2461 (51°45' N, 12° 55' W; 1153 m water depth), SU8118 (37° 46' N, 10°11'W; 3135 m water depth), OCE326-GGC5/ODP Site 1063 (33° 42' N, 57° 35'W; 4550 m water depth), and North Greenland Ice Core Project (NGRIP; 75° 5' N, 42° 17' W). EGC East Greenland Current, IC Irminger Current, LC Labrador Current, NAC North Atlantic Current. (b) Area shaded in white: LIS extent area shaded in green; IRD-belt in the North Atlantic16; HS Hudson Strait. This map was generated with Ocean Data View.

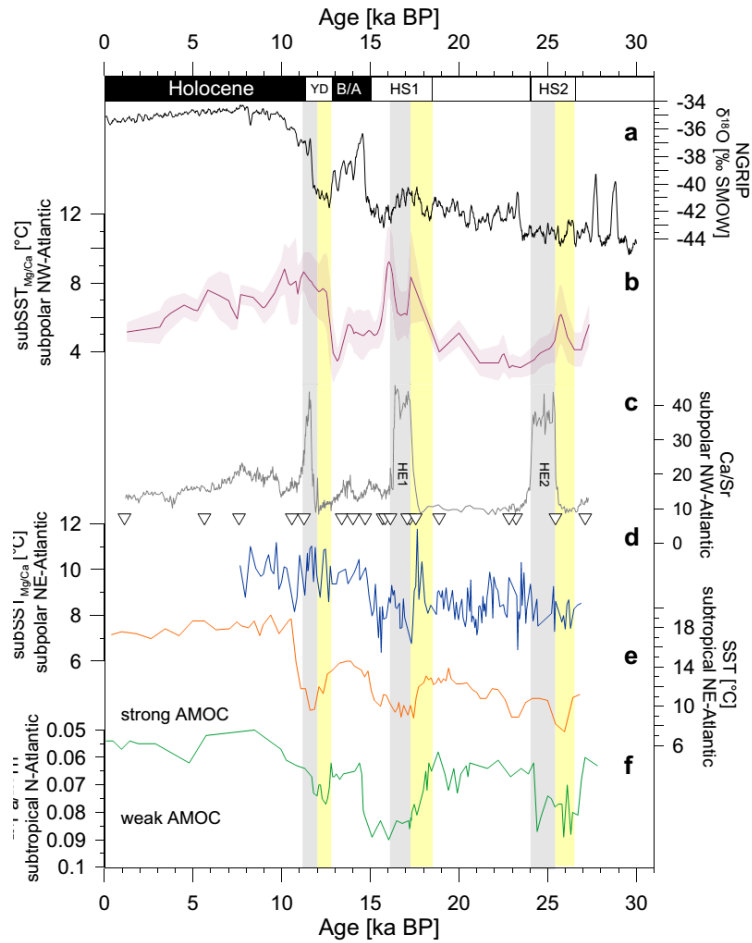


Figure 2. Comparison of proxy records from sediment core GeoB18530-1 to representative Greenland– North Atlantic proxy records over the last 27,000 years. a North Greenland Ice Core Project (NGRIP) stable oxygen isotopic composition ($\delta^{18}\text{O}$) reflecting atmospheric temperatures over Greenland. b Mean ages from age model ensemble for subsurface temperatures of core GeoB18530-1 with 95% confidence interval (this study). c X-ray fluorescence scanning-derived calcium to strontium ratios (Ca/Sr) (grey line) and age control points derived from calibrated AMS ^{14}C ages (open triangles) from core GeoB18530-1 (this study). d Subsurface temperatures from core MD01-2461 (eastern subpolar North Atlantic). e Alkenone sea surface temperatures from core SU8118 (eastern subtropical North Atlantic). f Pa/Th ratio reflecting the strength of the Atlantic Meridional Overturning Circulation (AMOC). Time series from 0 to 19 ka BP derived from core OCE326-GGC56, time series from 20 to 27 ka BP derived from ODP Site 106326. Yellow bars = phases of increases in subSSTMg/Ca into Heinrich Events and the Younger Dryas (YD); grey bars = Heinrich Layers (HE2 Heinrich Event 2, HE1 Heinrich Event 1) and the YD. B/A Bølling–Allerød interstadial, HS Heinrich Stadials.

2. 埃特纳火山灰岩石磁学特征

翻译人: 张琪 zhangq7@sustech.edu.cn



Vigliotti L, Bilardello D, Winkler A, et al. *Rock magnetic fingerprint of Mt Etna volcanic ash* [J] *Geophysical Journal International*, 2022, 231, 2, 749-769.

<https://doi.org/10.1093/gji/ggac213>

摘要: 本文对意大利埃特纳火山爆发活动中不同类型喷发产物的火山灰样品并进行了详细的岩石磁性研究, 用来测试应用磁性特性作为区分因素, 特别是对喷发属性进行区分。样品包括过去 18 ka 的侵入火山碎屑: benmoretic (一种粗粒岩) 来自更新世 Ellittico 火山活动的 Plinian 式火山喷发海洋岩芯 ET97-70 (爱奥尼亚海); 玄武岩来自全新世 FG 火山喷发(公元前 122 年); 火山坡面收集的 Strombolian/Phreatomagmatic/Sub-Plinian 式火山喷发样品(即全新世 TV、FS、FL、ETP 喷发的产物以及 1990 年、1998 年火山喷发), 和最近的 2001-2002 年发生的侧翼喷发活动样品(熔岩泉称为“Ash Rich Jets and plume”, 简称 ARJP)。Mössbauer 谱分析表明, 单一的磁性矿物主导了以上三组样品, 具有不同的磁性颗粒大小和组成特征。详细的岩石磁性研究包括低温、高温剩磁和磁化率测量, 表明 Plinian 式火山爆发和 ARJP 式活动火山喷发的喷出产物为氧化的含钛磁铁矿, 居里温度在 230 ~ 330°C 之间。FG 和 ARJP 火山碎屑总体上具有较高的矫顽力分布, 以及较高的磁化强度和磁化率, 包括在室温以下。相反, 大多数 Strombolian/sub-Plinian 样品磁性特征显示, 主要由矫顽力低的磁铁矿和/或贫钛-钛磁铁矿组成。晚更新世和全新世 Plinian 式火山喷发产物的磁性差异可以归因于前者喷发的成分不同, 后者是由进一步演化了的岩浆提供的, 而过去几十年火山喷发产物的地球化学变化可以解释全新世和最近的 Strombolian/sub-Plinian 产物之间的差异。大多喷发产物所包含的玄武玻璃碎屑的详细磁学特征研究, 认定玄武玻璃是 Plinian FG 和 ARJP 碎屑中磁信号的来源, 可能是冷却过程造成的。此外, 以上这些喷发形式产生的大量超顺磁性颗粒, 被认为可以用来表示 nanolite 组成, 是造成岩浆粘度增加的原因, 同时也是使它们具有喷发特征的原因。含玄武玻璃碎屑的独特岩石磁学特征, 可以用来表示区别于大部分喷发活动的粉碎过程, 这为研究火山学提供了一种十分有用的磁学方法。

ABSTRACT: A detailed rock magnetic study was conducted on ash samples collected from different products erupted during explosive activity of Mount Etna, Italy, in order to test the use of magnetic properties as discriminating factors among them, and their explosive character in particular. Samples include tephra emplaced during the last 18 ka: the benmoreitic Plinian eruptions of the Pleistocene Ellittico activity from marine core ET97-70 (Ionian Sea) and the basaltic Holocene FG eruption (122 BC), the Strombolian/Phreatomagmatic/sub-Plinian eruptions (namely, the Holocene TV, FS, FL, ETP products and the 1990, 1998 eruptions) collected from the slope of the volcano, and the Recent explosive activity (lava fountains referred to as ‘Ash Rich Jets and Plumes’, or ARJP) that occurred in the 2001–2002 period, related to flank eruptions. Mössbauer spectrometry informs that a single magnetic mineral dominates the three groups, which are characterized by variable magnetic grain sizes and composition. Detailed rock-magnetic investigations, ranging from low temperature to high temperature remanence and susceptibility experiments, indicate that the more explosive products of the Plinian eruptions and ARJP activity tephra, are characterized by oxidized Ti-rich titanomagnetites, with dominant Curie Temperatures between 230 and 330 °C. The FG and ARJP tephra are also characterized by contrasting, yet overall higher, coercivity distributions and higher magnetizations and susceptibilities, including below room temperature. In contrast, most of the Strombolian/sub-Plinian eruptions have a magnetic signature dominated by less coercive magnetite and/or Ti-poor titanomagnetite. Magnetic differences observed between the Late Pleistocene and Holocene FG Plinian eruptions can be attributed to the different composition of the former eruptions, which were fed by more evolved magmas, whereas geochemical variations characterizing the products erupted in the last few decades can be responsible for the differences between the Holocene and recent Strombolian/sub-Plinian products. Importantly, detailed magnetic investigation of sideromelane and tachylite clasts, the two end members of the juvenile fraction extracted from the ash of the most explosive products, determines that the tachylite fraction is responsible for the magnetic signature of the Plinian FG and ARJP tephra, and is attributed to the intense fragmentation that characterizes these activities, likely resulting from undercooling processes. Moreover, the abundant superparamagnetic grains associated with these eruptive styles are believed to represent the nanolite fraction responsible for the increasing viscosity of these magmas, and to be responsible for their explosive character. The distinctive magnetic properties that characterize the tachylite-bearing tephra, representative of the

fragmentation process that distinguishes the most explosive activities, provides a useful magnetic tool that can complement traditional volcanological investigations.

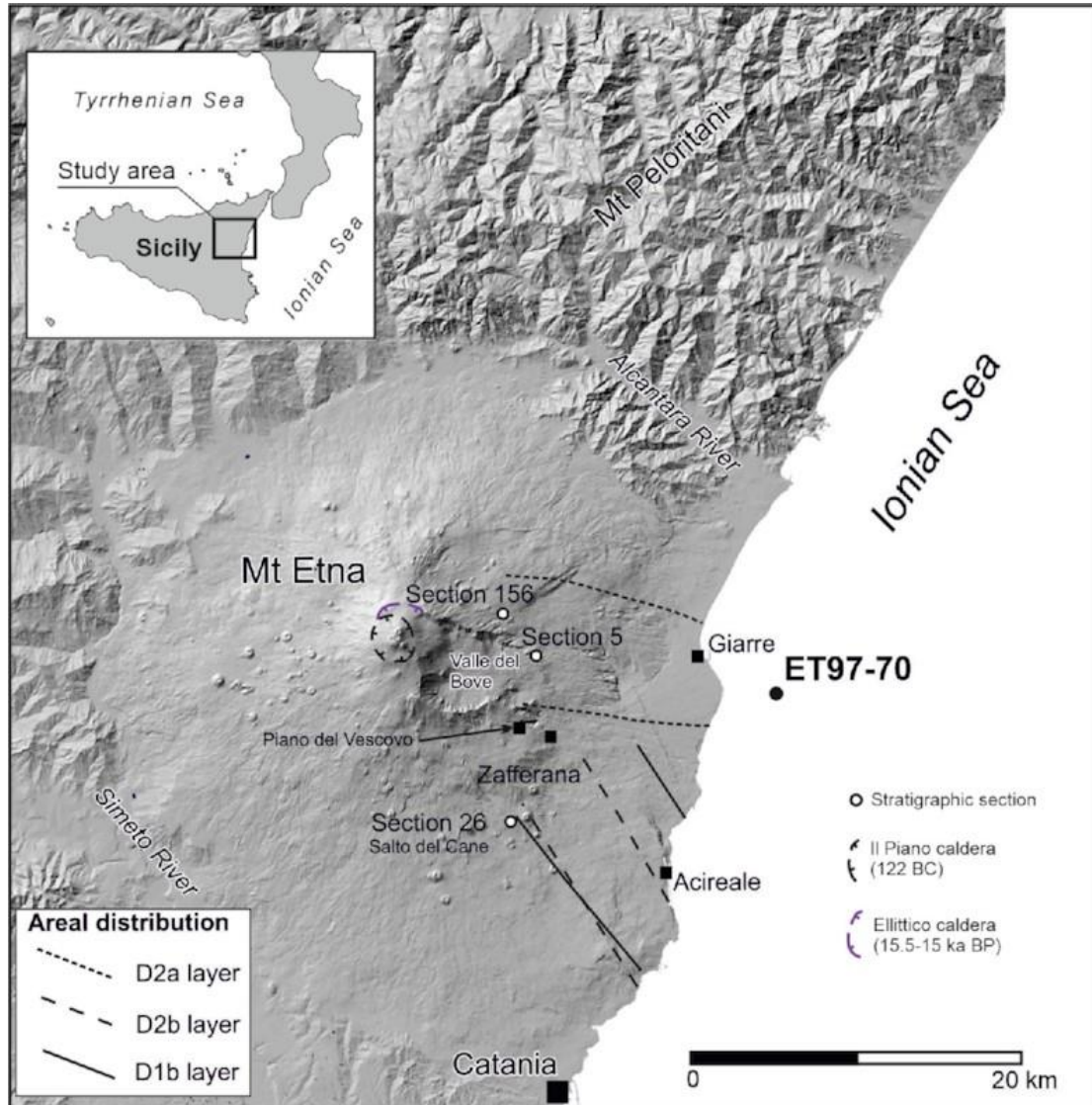


Figure 1. Map of the Etna region with the location of the studied samples.

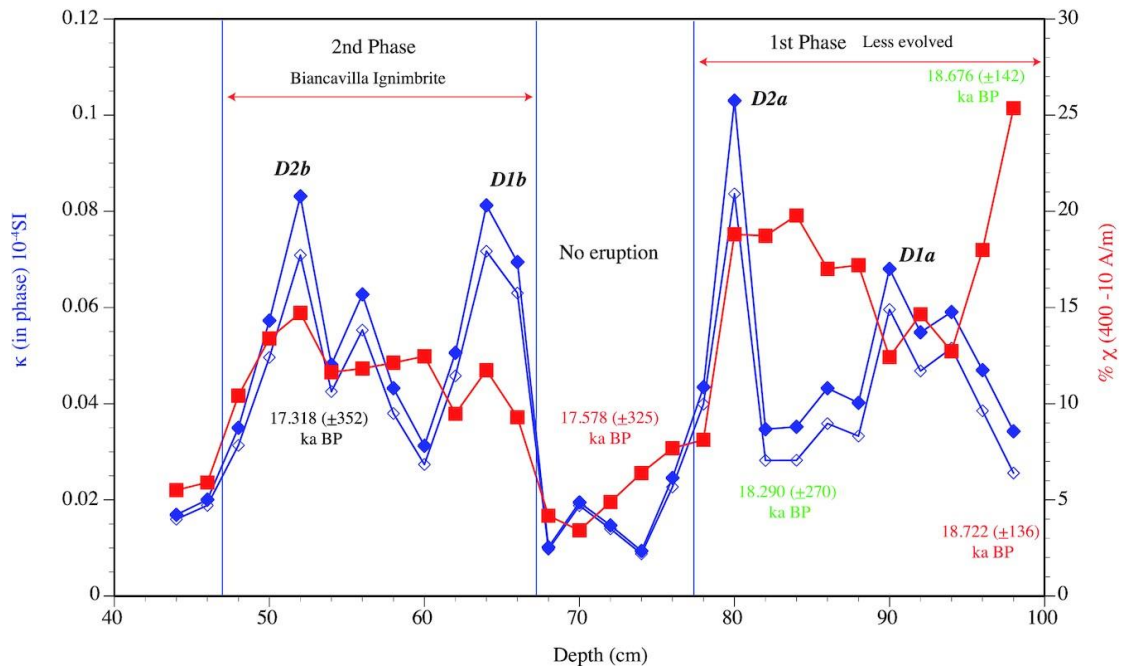


Figure 2. Magnetic susceptibility data of samples from Core ET97-70 (Late Pleistocene tephra). Blue symbols refer to in-phase susceptibility at different alternating field amplitudes: 10 Am^{-1} (open symbols) and 400 Am^{-1} (solid symbols). Red squares refer to the percentage of amplitude-dependence of the susceptibility between the two applied fields. The ages reported in the plot represent datings of the eruptions published by different authors: Albert et al. (2013) (black colour), Coltelli et al. 2000 (Green colour), Vigliotti et al. 2011 (red colour).

3. 碰撞引发的俯冲起始:基于实例和模型的综述

翻译人: 刘伟 ineway@163.com



Yang G. Subduction initiation triggered by collision: A review based on examples and models [J]

Earth-Science Reviews, 2022, 104129.

<https://doi.org/10.1016/j.earscirev.2022.104129>

摘要: 俯冲起始是板块构造理论中尚未解决的主要问题之一,提出的机制各不相同。在弧(海台、地体)-大陆碰撞模式中,俯冲极性反转或俯冲迁移可诱导一个新的俯冲带。本文综述了极性反转和俯冲迁移导致的典型俯冲起始的自然实例和数值模型,总结了俯冲起始的关键特征、地质记录和未来的研究方向。俯冲极性反转通常发生在洋内弧环境,而俯冲转移则经常发生在活动大陆边缘和洋内弧环境。俯冲极性反转和俯冲迁移的自然实例中有代表性的俯冲带上蛇绿岩(SSZ型蛇绿岩-蛇绿混杂岩)和变质底岩的地质记录,它们分别是上板块伸展和下板块埋藏的岩石记录,长期以来被认为是理解俯冲起始和地球动力学过程的关键。在自然观测和数值模型中,碰撞诱导的俯冲极性逆转和俯冲迁移通常发生在碰撞后 10 Myr 左右,需要薄弱区和驱动力。然而,在原特提斯洋、古特提斯洋和新特提斯洋碰撞后约 10-30 Myr 发生俯冲迁移。由二维向三维转变的俯冲起始数值模型可以突破二维几何模型的约束,更好地模拟俯冲起始过程。然而,数值模拟中所使用的参数还不能完全描述俯冲起始的各种控制因素。此外,弱流变性作用的机理及其对俯冲起始的影响仍不明确,需要通过自然观测和数值模拟进一步加以研究。

ABSTRACT: Subduction initiation is one of the main unsolved issues in plate tectonics theory with different proposed mechanisms. In the arc (plateau, terrane)-continent collision models, a new subduction zone can be induced by subduction polarity reversal or subduction transference. In this study, I have reviewed the typical natural examples and numerical models for the subduction initiation of polarity reversal and subduction transference, and then summarized the key characteristics, geological records, and future directions of the subduction initiation. The subduction polarity reversal usually occurs at intraoceanic arc settings, but the subduction transference often happens at active continental margins as well as intraoceanic arc settings. Natural examples of

subduction polarity reversal and subduction transference have representative geological records of supra-subduction zones (SSZ) ophiolites (ophiolitic mélanges) and metamorphic soles, which have long been recognized as the key to understanding the subduction initiation and geodynamic processes, because both are rock records of upper plate extension and lower plate burial, respectively. Weak zones and driving forces are required for the collision-induced subduction polarity reversal and subduction transference, which generally occurs about 10 Myr after collision both in natural observations and numerical models. However, subduction transference happens about 10–30 Myr after the collision in the Proto-, Paleo-, and Neo-Tethys oceans. Numerical models of the subduction initiation moving from 2D to 3D will break through the constraints of the 2D geometric model and better simulate the subduction initiation processes. However, the parameters used in the numerical modelling are not yet able to fully describe the various controlling factors of the subduction initiation. Moreover, the mechanism of weak rheology and its effect on the subduction initiation are still ambiguous and need further study by natural observations and numerical modelling.

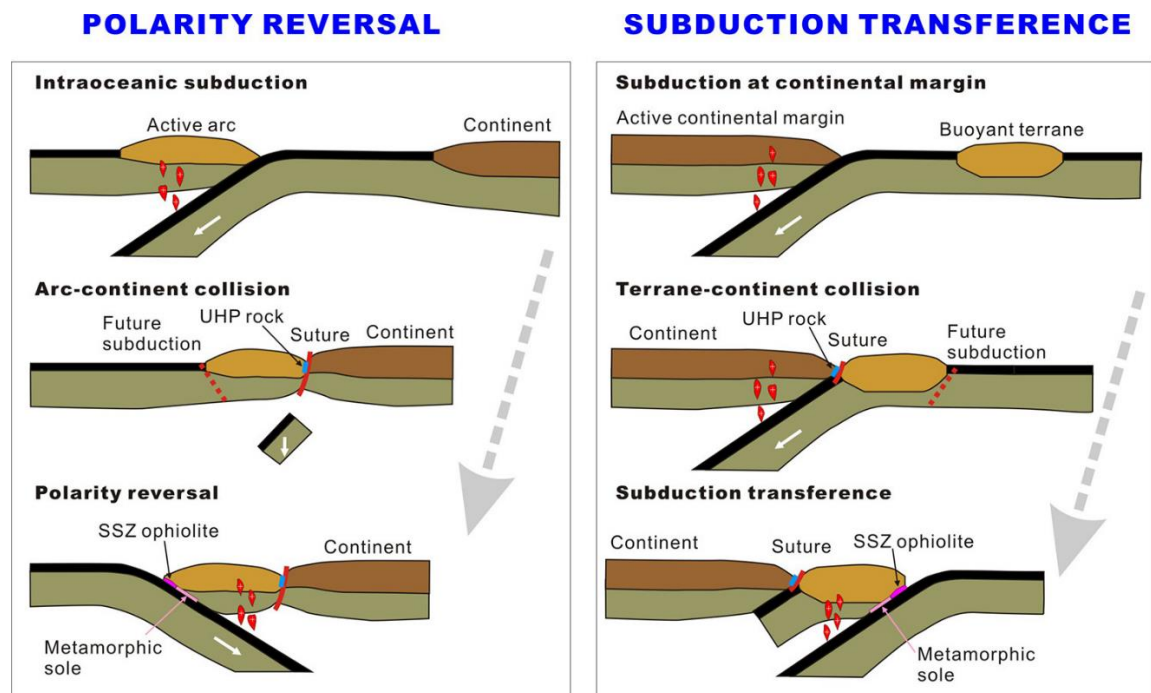


Figure 1. Cartoon showing geodynamic models of subduction initiation (inspired by Stern, 2004):

(a) Subduction polarity reversal, (b) Subduction transference.

4. 过去 2000 年东亚-太平洋模式和 ENSO 对长江流域中部百年尺度水文气候变化的调制



翻译人：杨会会 11849590@mail.sustech.edu.cn

Zhang J W, Zhao K, Wang Y J, et al. *Modulation of centennial-scale hydroclimate variations in the middle Yangtze River Valley by the East Asian-Pacific pattern and ENSO over the past two millennia* [J] *Earth and Planetary Science Letters*, 2021, 576, 117220.

<https://doi.org/10.1016/j.epsl.2021.117220>

摘要：气象观测结果显示，在年际和季内时间尺度上，热带西北太平洋(WNP)和长江流域中部(YRV 中部)夏季风降水呈反比关系。这种被称为东亚-太平洋(EAP)的跷跷板型模式，是影响长尾湖中部夏季降水的主要遥相关因素之一。然而，由于缺乏长时间连续的观测数据，人们对长时间尺度上的 EAP 模式的行为和机制知之甚少。本文根据神奇洞内两颗石笋(EB1 和 EB5) 1221 个 $\delta^{18}\text{O}$ 数据和 22 个 ^{230}Th 定年数据，建立了公元前 230 年至公元 1810 年的高分辨率综合夏季风降水记录。我们的新记录显示，YRV 中部的季风降水以约 100 年的主要周期变化，这可能与太阳活动和 ENSO 变率有关。该记录与附近的和尚洞和落水洞的两个石笋 $\delta^{18}\text{O}$ 记录具有很强的相似性，与北半球温度重建结果基本一致。为了反映长江下游三个洞穴 $\delta^{18}\text{O}$ 记录的综合水文气候变化特征，利用主成分分析方法提取了三个洞穴 $\delta^{18}\text{O}$ 记录的第一主成分(PC1)。结果表明，YRV 中部与 WNP 之间的干湿关系显著相反，EAP 模式的变化对百年尺度季风降水变化具有重要影响。此外，我们还利用 YRV 中部和 WNP 的季风降水记录，重建了一个新的 EAP 指数。该 EAP 指数与 ENSO 指数具有很强的相关性，证实 ENSO 变率可能通过 EAP 遥相关在调节 YRV 中部的季风降水中发挥关键作用。

ABSTRACT: Meteorological observations reveal an inverse relationship of summer monsoon rainfall between the tropical western North Pacific (WNP) and middle Yangtze River Valley (mid-YRV) on interannual and intraseasonal timescales. This seesaw-like pattern, named the East Asian-Pacific (EAP) pattern, is one of the major teleconnections that affect summer precipitation in the mid-YRV. However, due to the scarcity of long and continuous instrumental data, the behavior and mechanism of the EAP pattern on a long timescale are poorly understood. Here, we present a

composite high-resolution summer monsoon rainfall record from 230 BC to 1810 AD, based on 1221 $\delta^{18}\text{O}$ measurements and 22 ^{230}Th dates from two stalagmites (EB1 and EB5) in Shenqi Cave over the mid-YRV. Our new record shows that monsoon rainfall in the mid-YRV varies at a dominant periodicity of ~ 100 years, probably linked to solar activity and ENSO variability. The multi-centennial fluctuations in the EB record, broadly consistent with the North Hemisphere temperature reconstruction, display strong similarities to two stalagmite $\delta^{18}\text{O}$ records from nearby Heshang and Luoshui caves. To represent the integrated hydroclimate variations over the mid-YRV, we extracted the first principal component (PC1) of these three cave $\delta^{18}\text{O}$ records by using the principal component analysis. We reveal a striking inverse relationship of wet/dry conditions between the mid-YRV and tropical WNP, suggesting that changes in the EAP pattern have an important impact on centennial-scale monsoon precipitation changes. Furthermore, we compile monsoon rainfall records from the mid-YRV and WNP to reconstruct a new EAP index. This EAP index exhibits a strong correlation with the ENSO proxy, confirming that the ENSO variability may play a key role in modulating the monsoon rainfall in the mid-YRV through the EAP teleconnection.

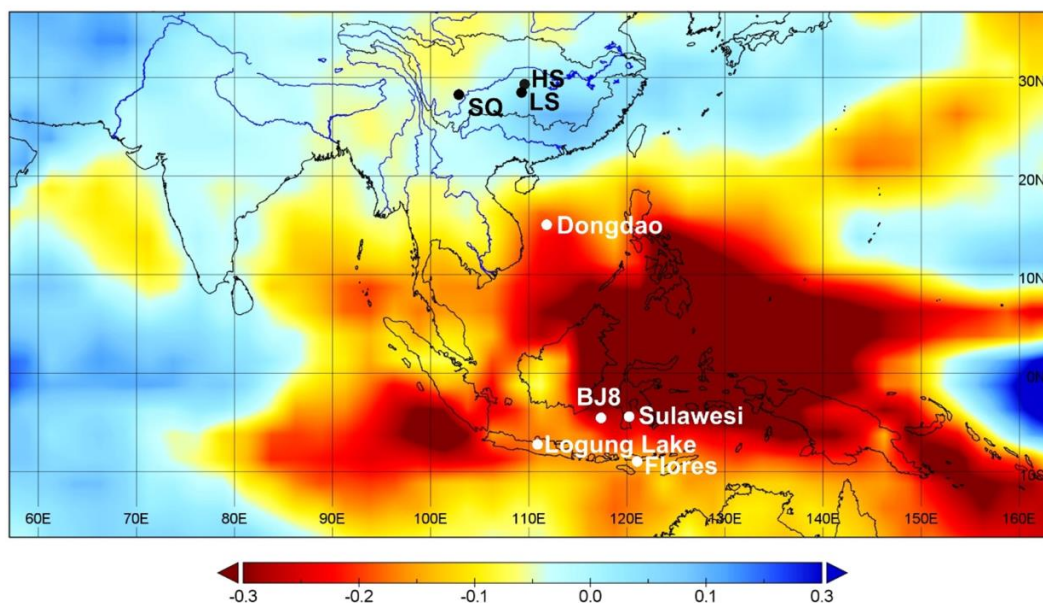


Figure 1. Correlation between Nino 3.4 sea surface temperature and summer (June-July-August) rainfall anomalies in tropical WNP and East Asia (research data is available at: <http://research.jisao.washington.edu/data/gpcp/>). The study sites, mentioned in the text, are illustrated: Shenqi Cave (SQ, this study), Heshang Cave (HS, Hu et al., 2008), Luoshui Cave (LS, Xue et al., 2020),

Cattle Pond, Dongdao (Yan et al., 2011a), BJ8 core from the Makassar Strait (Oppo et al., 2009), marine sediments from the Sulawesi (Tierney et al., 2010), Lake Logung, East Java (Rodysill et al., 2012), and Liang Luar Cave, southeastern Indonesia (Griffiths et al., 2016). (For interpretation of the colors in the figure(s), the reader is referred to the web version of this article.)

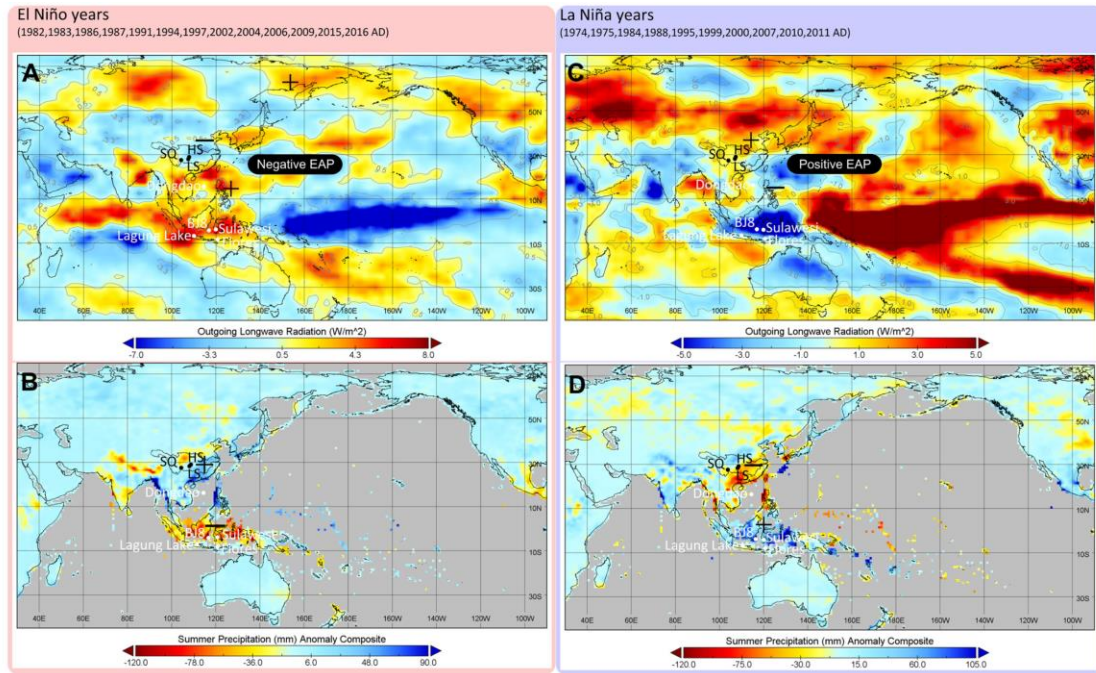


Figure 2. The impacts of the ENSO and EAP pattern on the summer rainfall (June-July-August, JJA) in the YRV since the 1970s. (A) Negative EAP pattern constructed by the composite OLR data during the typical El Niño years, (B) The spatial pattern of summer rainfall anomaly during the typical El Niño years, (C) Positive EAP pattern during the typical La Niña years, (D) The spatial pattern of summer rainfall anomaly during the typical La Niña years. Black and white dots indicate the study sites discussed in the text with the same labels as in Fig. 1. All meteorological data are available at: <https://www.esrl.noaa.gov/psd/cgi-bin/data/getpage.pl>.

5. 青藏高原东南部全新世中-晚期相对温暖的证据



翻译人：张靖宇 zhangjy6@sustech.edu.cn

Xiaoping Feng, Cheng Zhao, William J D, et al. Evidence for a relatively warm mid-to late Holocene on the southeastern Tibetan Plateau [J] Geophysical Research Letters, 2022.

<https://doi.org/10.1029/2022GL098740>

摘要： 在古气候重建和气候模型模拟之间的全新世温度差异，被认为是全新世温度的难题，需要在高海拔地区建立新的高质量全新世温度记录。这里，基于青藏高原东南部一个偏远和小的 高山湖泊的支链甘油二烷基甘油四醚校准，我们提出了一个定量的全新世年平均气温记录。该记录显示了一个温度历史，包括一个相对凉爽的全新世早期（7 ka 之前），然后是一个较温暖的全新世中-晚期（7 ka 之后），这可能与当地年日照量和温室气体（GHGs）的增加有关。三次降温事件打断了总的变暖趋势，分别为 10.4 ka、3.7 ka 和 1.7 ka，在时间上与北大西洋的冰筏事件以及火山活动和/或异常太阳活动的事件密切相关。整个全新世的温度比之前确定的 1990-2014 AD 人为变暖要低。

ABSTRACT: The Holocene temperature discrepancy between paleoclimate reconstructions and climate model simulations—known as the Holocene temperature conundrum—calls for new high-quality Holocene temperature records at high elevations. Here, we present a quantitative Holocene mean annual air temperature record based on a site-specific branched glycerol dialkyl glycerol tetraethers calibration from a small remote alpine lake on the southeastern Tibetan Plateau. The record reveals a temperature history comprising a relatively cool early Holocene (before 7 ka) followed by a warmer mid- to late-Holocene (after 7 ka), which was likely linked to increasing local annual insolation and greenhouse gases (GHGs). Three cold events punctuated the general warming trend ca. 10.4 ka, 3.7 ka, and 1.7 ka, and correspond closely in time to ice rafting events in the North Atlantic, and to episodes of volcanism and/or unusual solar activity. The entire Holocene temperatures are cooler than the previously identified anthropogenic warming from 1990-2014 AD.

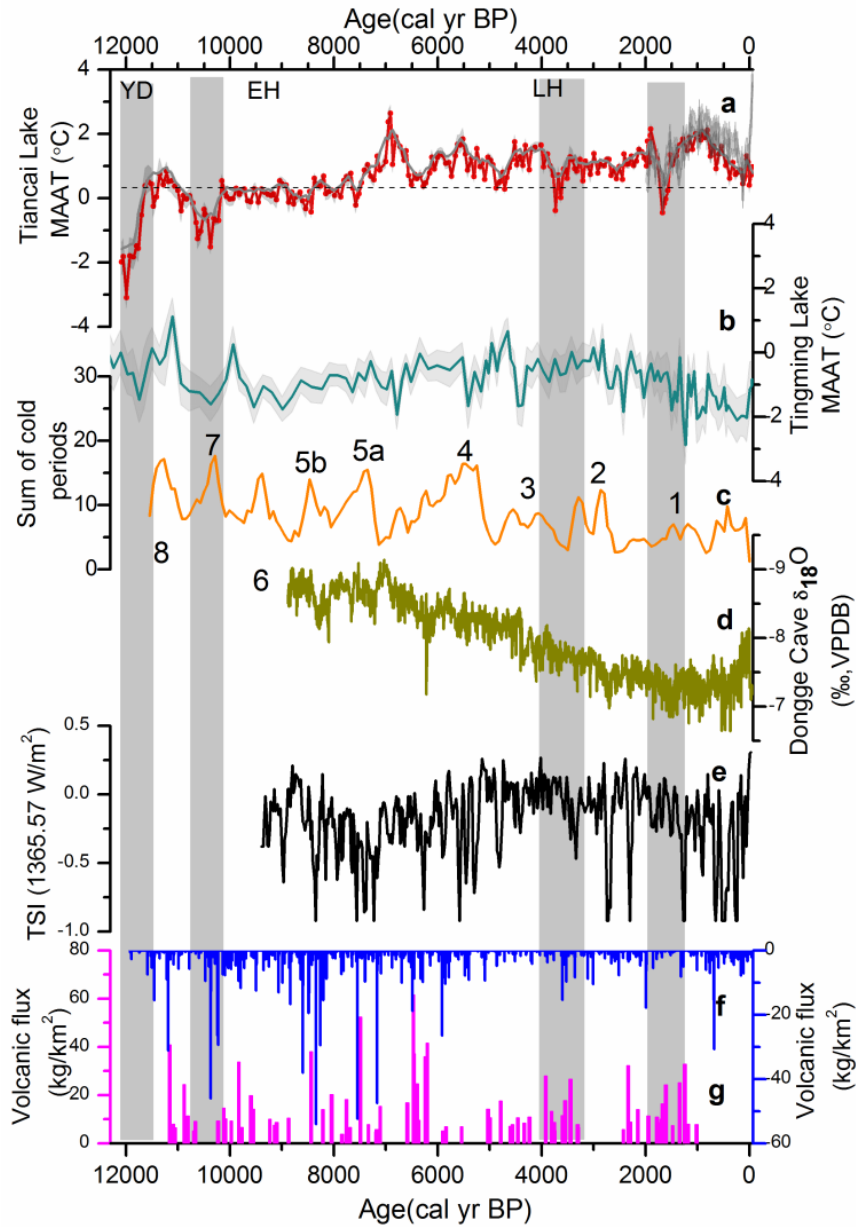


Figure 1. Centennial scale temperature fluctuations at Tiancai Lake. (a) brGDGT-inferred temperature record with $\pm 2\sigma$ uncertainty at Tiancai Lake, (b) brGDGT-recalculated MAAT record with $\pm 2\sigma$ uncertainty at Tingming Lake, (c) The orange curves with the numbers show the standardized ocean stacked ice rafted debris (IRD) record representing the Bond events No. (0-8) (Bond et al., 2001), (d) $\delta^{18}\text{O}$ time series of the Dongge Cave stalagmite DA (Wang et al., 2005), (e) Total solar Irradiance (Steinhilber et al., 2012), (f-g) volcanic activity (derived from Greenland GISP2 record (blue) and Antarctic Dome C record (red) (Castellano et al., 2005; Kobashi et al., 2017)). The gray vertical bars denote the cold events.

6. 中世纪气候异常期间的古环境条件、小冰期和中美洲东部地区的社会影响



翻译人: 王浩森 11930841@mail.sustech.edu.cn

Wogau K H, Hoelzmann P, Arz H W, Böhnelt, H N. *Paleoenvironmental conditions during the Medieval Climatic Anomaly, the Little Ice Age and social impacts in the Oriental Mesoamerican region [J]* *Quaternary Science Reviews*, 2022, 289, 107616.

<https://doi.org/10.1016/j.quascirev.2022.107616>

摘要: 中世纪气候异常和小冰期是过去 1000 年里最相关的气候事件。虽然之前的一些研究描述了对中美洲古环境条件的影响以及潜在的大气-海洋驱动因素, 但还需要更多的研究。虽然大多数古环境记录揭示了以干旱条件为主的中世纪气候异常, 但小冰期的古气候特征似乎更具争议。一些记录显示了普遍的干旱条件, 少数记录表明湿润条件。在这里, 我们展示了一个新的高分辨率古环境记录, 该记录来自位于东中美洲地区的 Serdan 东方盆地。我们采用了 Alchichica 火山口 maar 湖的部分分层沉积层序。通过微相分析、地球化学分析、矿物学成分和磁性分析进行了多参数研究。阿尔奇卡湖内生碳酸钙沉淀的增强表明了中世纪气候异常期间的主要干燥条件。另一方面, 小冰期代表了以湿润为主的条件的增强, 并被短时间的干旱间隔所打断。更潮湿的事件描述为 varve 保存增加、碎屑输入和碳酸钙沉淀减少。此外, 我们认为, 北大西洋涛动的可变性以及飓风活动可能影响了中美洲东部地区两种气候异常期间的水文模式。最后, 我们假设在中世纪气候异常期间记录的严重干旱条件, 包括后经典考古学时期, 对农业生活方式有用的两个重要景观要素有严重影响: El Salado 湖沼平原和 piedmonts。

ABSTRACT: The Medieval Climatic Anomaly and the Little Ice Age periods are the most relevant climatic events in the last 1000 yr BP. Although some research describes the effects on Mesoamerican paleoenvironmental conditions and the potential atmospheric-oceanic drivers involved, more studies are needed. While most paleoenvironmental records reveal a Medieval Climatic Anomaly dominated by arid conditions, the paleoclimatic signature of the Little Ice Age seems to be more controversial. Some records display prevailing drought conditions and a minor

number of records suggest wetter conditions. Here, we present a new high-resolution paleoenvironmental record from the Serdan Oriental Basin, located in the Oriental Mesoamerican region. We employed the partly laminated sedimentary sequence from the Alchichica crater maar lake. A multi-proxy study by means of microfacies analyses, geochemical analyses, mineralogical composition and magnetic analysis was conducted. Enhanced endogenic calcium carbonate precipitation in the Alchichica lake points to dominant dry conditions during the Medieval Climatic Anomaly. On the other hand, the Little Ice Age represented the rise of predominantly wetter conditions interrupted by short drought intervals. The wetter event is described by increased varve preservation, detrital input, and decreased calcium carbonate precipitation. Furthermore, we argue that the variability of the North Atlantic Oscillation in conjunction with hurricane activity could have influenced the hydrological patterns during both climatic anomalies in the Oriental Mesoamerican sector. Finally, we hypothesize that severe drought conditions registered during the Medieval Climatic Anomaly, which encompasses the Postclassic archeological period, had severe implications in two important landscape elements useful to the agriculture lifestyle: El Salado lacustrine plain and piedmonts.

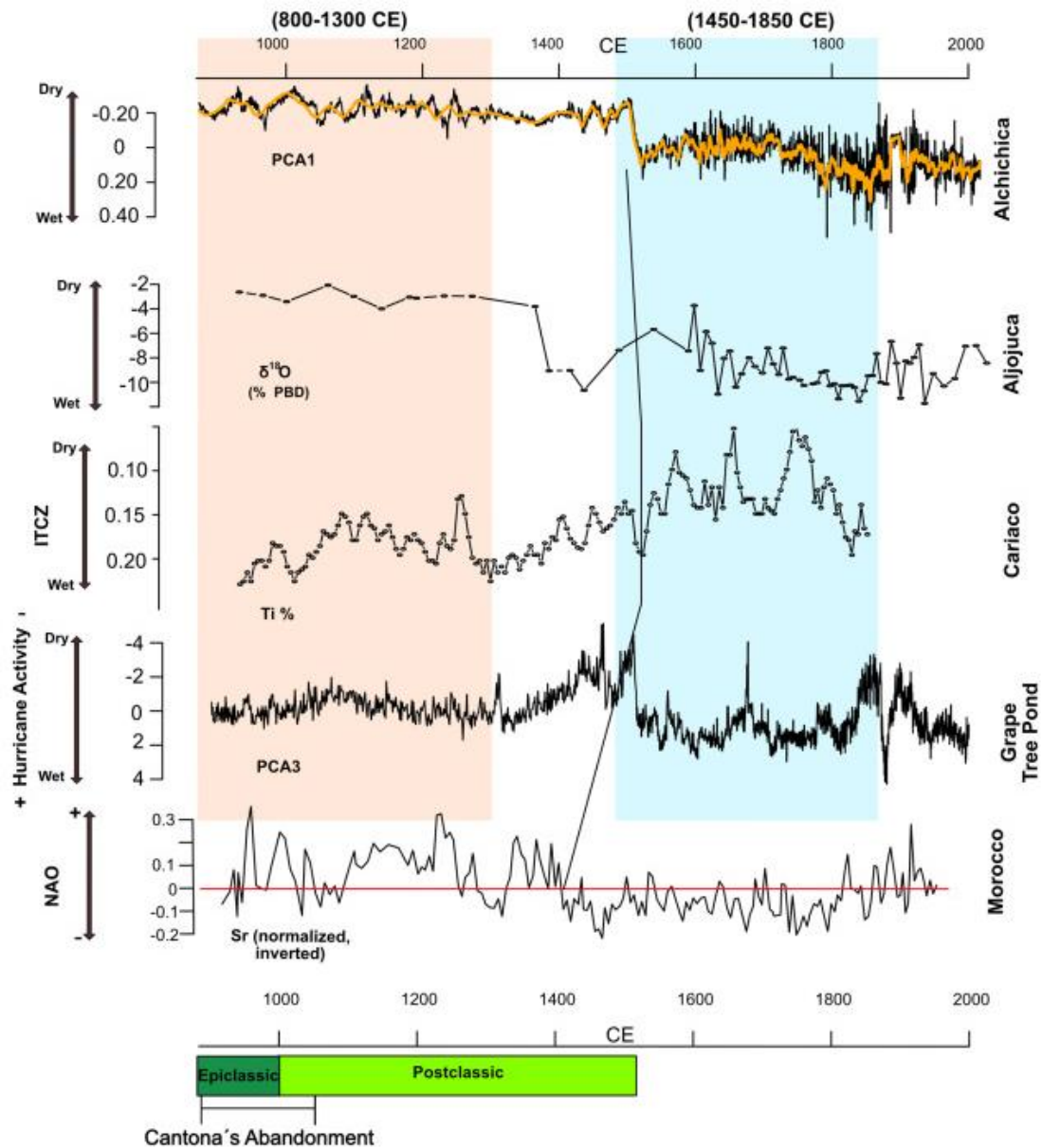


Figure 1. Four topographic sections and the main landscape features from the Northern Serdan Oriental Basin area. Purple shadings indicates the piedmont areas, blue shadings show the lacustrine plain and yellow shading indicates small towns.

7. 来自以色列北部更新世古强度结果: 时间平均地磁场半球不对称性的意义

翻译人: 张伟杰 12031188@mail.sustech.edu.cn



Tauxe L, Asefaw H, Behar N A, et al. Paleointensity Estimates from the Pleistocene of Northern Israel: Implications for hemispheric asymmetry in the time averaged field [J] Geochemistry, Geophysics, Geosystems, 2022.

<https://doi.org/10.1029/2022GC010473>

摘要: 通过 IZZI 形式的 Thellier-Thellier 实验和严格的筛选标准, 从以色列北部的 22 个采点获得了更新世 (0.012 ~ 2.58 Ma) 古地磁轴向偶极矩 (PADM) 为 $62.24 \pm 30.6 \text{ ZAm}^2$ 。对来自南极洲, 冰岛和夏威夷同时代的已有研究利用相同的数据筛选标准进行重新分析, 结果表明, 以色列北部的平均数据略高于冰岛 ($\text{PADM} = 53.8 \pm 23 \text{ ZAm}^2$, 51 个采点), 明显高于南极洲 ($\text{PADM} = 40.3 \pm 17.3 \text{ ZAm}^2$, 42 个采点)。此外, 夏威夷岩心 HSDP2 指示过去 50 万年的磁场强度 ($\text{PADM} = 76.7 \pm 21.3 \text{ ZAm}^2$, 59 个采点) 也高于以色列北部的数据。这些结果与 PINT 数据库 (www.pintdb.org) 筛选过的更新世结果指示北半球中纬度地区的平均强度高于南半球以及纬度高于 60° N 的地磁场强度。因此, 在高纬度发现的较弱磁场强度不能归因于时变偶极矩的时空采样不足或数据质量低。北半球中纬度地区的高场可能是由于地磁场中长期存在的非轴向偶极子成分, 其在不同经度不同时间发生了高场强事件。这一假说得到了全新世、100 kyr 和 500 万年预测的平均时间地磁场模型不对称性的支持。

ABSTRACT: Twenty-two sites, subjected to an IZZI-modified Thellier-Thellier experiment and strict selection criteria, recover a paleomagnetic axial dipole moment (PADM) of $62.24 \pm 30.6 \text{ ZAm}^2$ in Northern Israel over the Pleistocene (0.012 - 2.58 Ma). Pleistocene data from comparable studies from Antarctica, Iceland, and Hawaii, re-analyzed using the same criteria and age range, show that the Northern Israeli data are on average slightly higher than those from Iceland ($\text{PADM} = 53.8 \pm 23 \text{ ZAm}^2$, $n = 51$ sites) and even higher than the Antarctica average ($\text{PADM} = 40.3 \pm 17.3 \text{ ZAm}^2$, $n = 42$ sites). Also, the data from the Hawaiian drill core, HSDP2, spanning the last half million years ($\text{PADM} = 76.7 \pm 21.3 \text{ ZAm}^2$, $n = 59$ sites) are higher than those from Northern Israel. These results,

when compared to Pleistocene results filtered from the PINT database (www.pintdb.org) suggest that data from the Northern hemisphere mid-latitudes are on average higher than those from the southern hemisphere and than those from latitudes higher than 60°N. The weaker intensities found at high (northern and southern) latitudes therefore, cannot be attributed to inadequate spatio-temporal sampling of a time-varying dipole moment or low quality data. The high fields in mid-latitude Northern hemisphere could result from long-lived non-axial dipole terms in the geomagnetic field with episodes of high field intensities occurring at different times in different longitudes. This hypothesis is supported by an asymmetry predicted from the Holocene, 100 kyr, and five million year time-averaged geomagnetic field models.

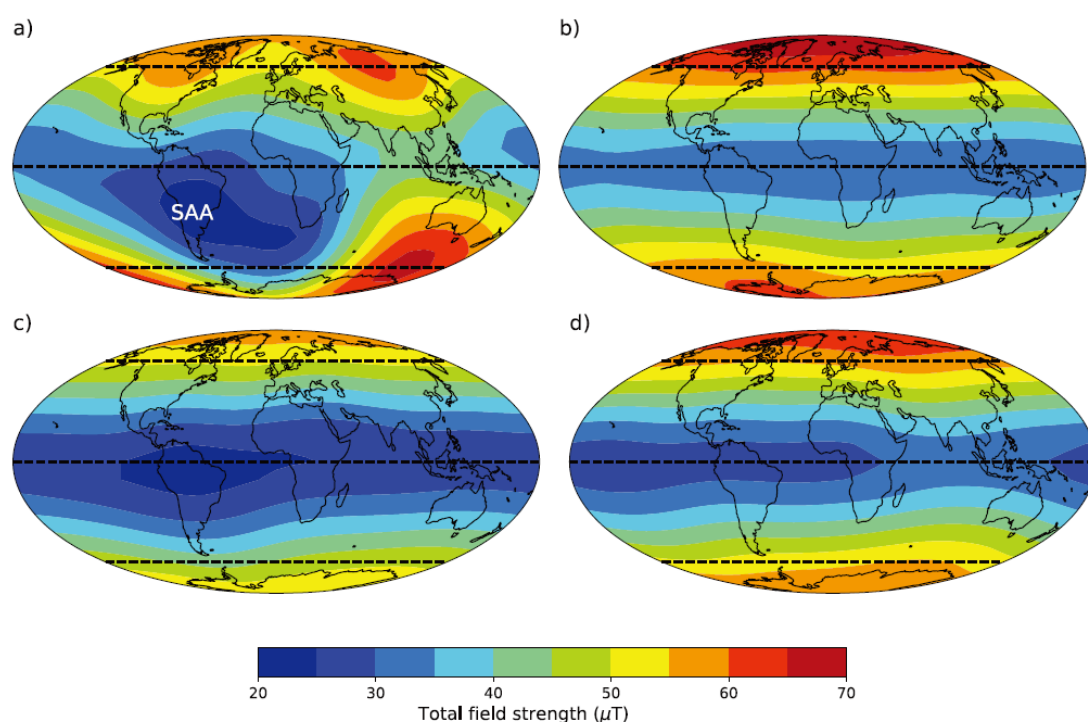


Figure 1. Intensity (in μT) of the geomagnetic field from global field models. a) International Geomagnetic Reference Field (IGRF) for the year 2022 (Alken et al., 2021). b) Average of the Holocene field from CALS10k.2 (Constable et al., 2016). c) Average field for the last 100ka (Panovska et al., 2018). d) LN3 time averaged field model for the last 5 Ma (Cromwell et al., 2018).

8. 晚中新世冷却与二氧化碳耦合具有类似更新世的气候敏感性

翻译人: 李海 12031330@mail.sustech.edu.cn



Brown R M, Chalk T B, Crocker A J, et al. *Late Miocene cooling coupled to carbon dioxide with Pleistocene-like climate sensitivity* [J] *Nature Geoscience*, 2022.

<https://doi.org/10.1038/s41561-022-00982-7>

摘要: 从 1200 万年前到 500 万年前的晚中新世, 地球气候明显变冷, 对全球生态系统产生了深远的影响。然而, 这些变化的驱动力仍然存在争议。其中温室气体辐射强迫所起的作用不确定是其主要制约因素。本文中, 作者展示了晚中新世的浮游有孔虫的硼同位素记录, 涵盖了 7~5 Ma 晚中新世冷却事件中最快速冷却时期的二氧化碳变化。研究结果表明, 在 200 万年的时间间隔中, 二氧化碳下降了约 100 ppm, 最低点约在 5.9 Ma 左右。考虑到非 CO₂ 温室气体和缓慢的气候反馈, 作者根据 CO₂ 辐射强迫记录和全球平均地表温度变化记录比较, 作者估计全球平均地表温度变化为二氧化碳的两倍--平衡气候敏感性为 3.9 °C (1.8~6.7 CO₂ 在 95%置信度下)。由此可得, 在最晚的中新世期间, 二氧化碳和气候的变化密切耦合, 平衡气候敏感性在政府间气候变化专门委员会提出的晚更新世、新生代和 21 世纪其他时间段的估计范围内。

ABSTRACT: Earth's climate cooled markedly during the late Miocene from 12 to 5 million years ago, with far-reaching consequences for global ecosystems. However, the driving forces of these changes remain controversial. A major obstacle to progress is the uncertainty over the role played by greenhouse gas radiative forcing. Here we present boron isotope compositions for planktic foraminifera, which record carbon dioxide change for the interval of most rapid cooling, the late Miocene cooling event between 7 and 5 Ma. Our record suggests that CO₂ declined by some 100 ppm over this two-million-year-long interval to a minimum at approximately 5.9 Ma. Having accounted for non-CO₂ greenhouse gasses and slow climate feedbacks, we estimate global mean surface temperature change for a doubling of CO₂--equilibrium climate sensitivity--to be 3.9 °C (1.8-6.7 °C at 95% confidence) on the basis of comparison of our record of radiative forcing from CO₂ with a record of global mean surface temperature change. We conclude that changes in CO₂ and

climate were closely coupled during the latest Miocene and that equilibrium climate sensitivity was within range of estimates for the late Pleistocene, other intervals of the Cenozoic and the twenty-first century as presented by the Intergovernmental Panel on Climate Change.

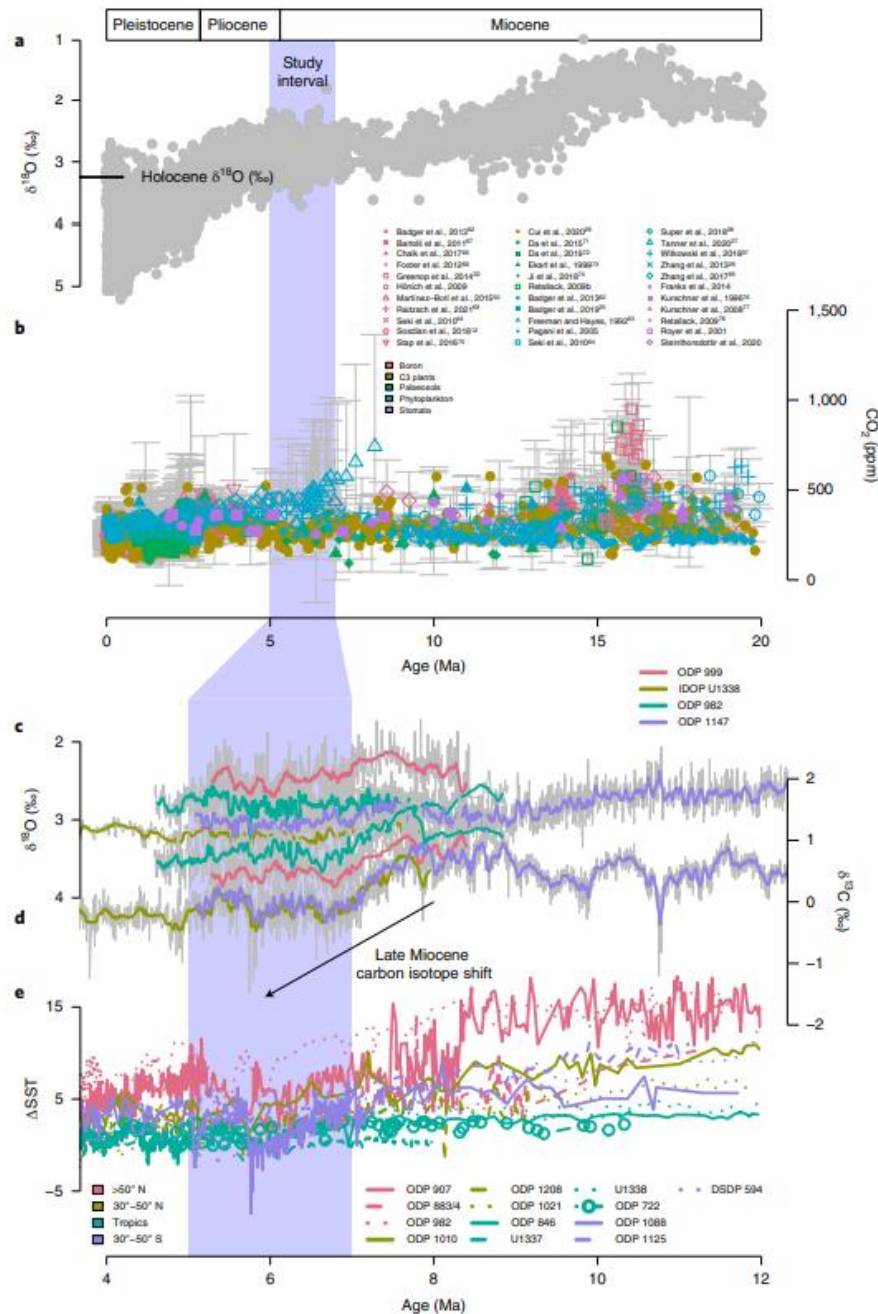


Figure 1. Neogene and late Miocene climate changes. a, Benthic foraminifera $\delta^{18}\text{O}$ stack for the Neogene⁶¹. b, Collection of published CO_2 estimates for the past 20 Myr using phytoplankton ($\delta^{13}\text{C}$ of phytoplankton compounds, blue)^{13,25,26,27,37,38,62,63,64,65,66}, boron isotopes of phytoplankton compounds, blue)^{13,25,26,27,37,38,62,63,64,65,66}, boron isotopes (orange)^{12,32,50,62,64,67,68,69,70,71,72}, C_3 plants (green)²⁹, palaeosols (teal)^{73,74,75,76,77} and stomata

(purple)^{78,79,80,81,82,83}. Error bars denote reported 2 s.d. Data compilation built on previous CO₂ compilation by ref.35. c,d, Twenty-point running mean $\delta^{18}\text{O}$ (c) and $\delta^{13}\text{C}$ (d) of benthic foraminifera records from ODP (Ocean Drilling Project) 999 (green)⁸⁴, IODP (International Ocean Drilling Project) U1338 (light blue)²², ODP 982 (red)⁴⁰ and ODP 1147 (dark blue)²¹. An equilibrium correction (+0.64‰) applied to all $\delta^{18}\text{O}$ records^{85,86}. e, SST records used in late Miocene temperature stack recalibrated using BAYSPLINE⁴³. Records are coloured according to latitude: >50° N, pink¹⁶; 30–50° N, yellow¹⁶; the tropics, green^{16,87,88,89}; 30–50° S, purple¹⁶. Site information and citations for all datasets are available in Supplementary Table 1.

9. 南大西洋福克兰群岛晚冰期—全新世南半球西风变化记录



翻译人：张亚南 zhangyn3@mail.sustech.edu.cn

Monteath A, Hughes P, Cooper M, et al. *Late glacial–Holocene record of Southern Hemisphere westerly wind dynamics from the Falkland Islands, South Atlantic Ocean* [J] *Geology*, 2022, 50(8), 880-885.

<https://doi.org/10.1130/G49805.1>

摘要：南半球西风带（SHWW）是南半球中纬度气候的一个主要特征，与南大洋二氧化碳封存和释放密切相关。但对过去西风带强度和位置变化的认识还很匮乏，特别是在更新世—全新世过渡时期，该时期与大气二氧化碳和温度波动相关。文中，作者利用南大西洋福克兰群岛泥炭沉积层中的风尘地球化学、粒度测量和古生态学分析，描述了 16.0 和 16.5 ka 时期 SHWW 的变化。南极冷逆转前后（ACR，14.9-13.0 ka）在 51°S 风强度较低，在 13.1-12.1 ka 随着大气温度升高而增强，随后减弱，并在早全新世暖期达到最低。在 12-10.2 ka 西北方气团占主导地位，直到 7.8ka 受到风暴潮或海啸影响，期间风力一直较弱。这些数据表明，在 ACR 期间 SHWW 从 51°S 以北向南进行纬向移动，全新世到达 51°S，早全新世暖期达到 51°S 以南。这种模式表明，在更新世—全新世的转变过程中，SHWW 与大气温度紧密耦合。

ABSTRACT: The Southern Hemisphere westerly wind belt (SHWW) is a major feature of Southern Hemisphere, midlatitude climate that is closely linked with the sequestration and release of CO₂ in the Southern Ocean. Past changes in the strength and position of this wind belt are poorly resolved, particularly across the Pleistocene-Holocene transition, a time period associated with fluctuations in atmospheric temperatures and CO₂ levels. We used dust geochemistry, particle size measurements, and paleoecological analyses from a peat sequence in the Falkland Islands, South Atlantic Ocean, to describe changes in the SHWW between 16.0 and 6.5 ka (thousands of years before CE 1950). Wind strength was low at ~51°S before and during the Antarctic Cold Reversal (ACR, 14.9–13.0 ka), intensified between 13.1 and 12.1 ka as atmospheric temperatures increased, and then weakened, reaching a minimum between 12.1 and 10.9 ka during the Early Holocene thermal maximum.

Northwesterly air masses became more dominant from 12.0 to 10.2 ka, and wind strength remained low until our record was affected by a storm surge or tsunami ca. 7.8 ka. These data indicate a southward shift in the latitude of the SHWW, from north of 51°S prior to and during the ACR, at ~51°S before the onset of the Holocene, and south of 51°S during the early Holocene thermal maximum. This pattern suggests that the latitude of the SHWW was coupled with atmospheric temperatures through the Pleistocene-Holocene transition.

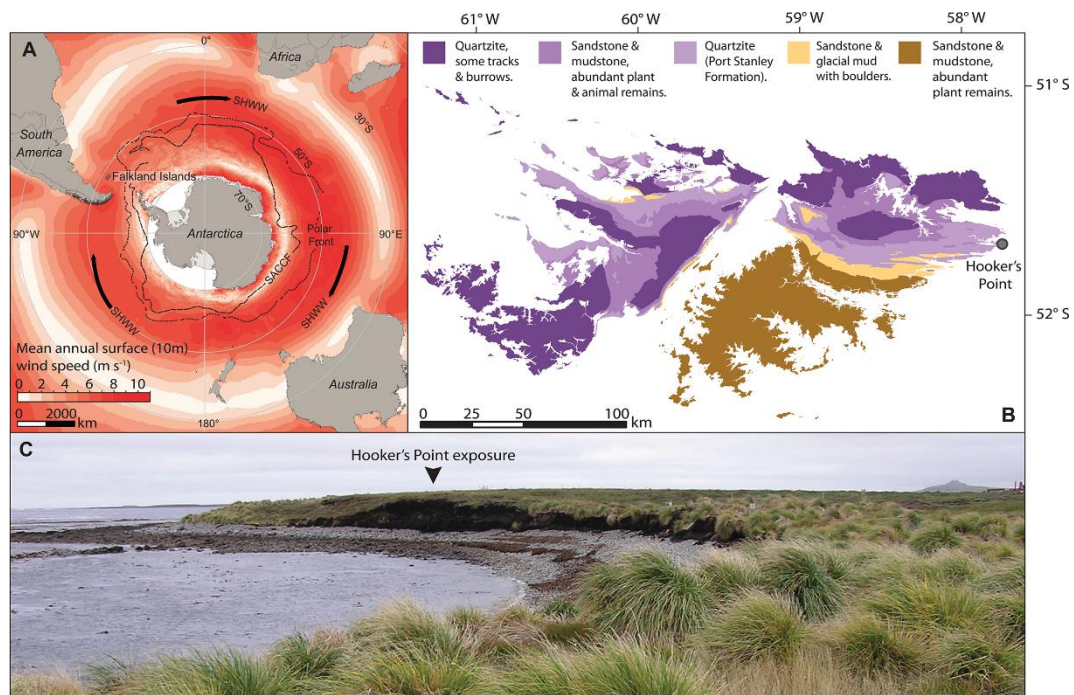


Figure 1. (A) Position of the Falkland Islands within the Southern Hemisphere westerly wind belt (SHWW). Shaded wind speeds are based on National Oceanic and Atmospheric Administration (NOAA) blended vector data (<https://www.ncdc.noaa.gov/data-access/marineocean-data/blended-global/blended-sea-winds>). SACCF—Southern Antarctic Circumpolar Current Front. (B) Geologic formations in the Falkland Islands. (C) Hooker's Point exposure and surrounding landscape.

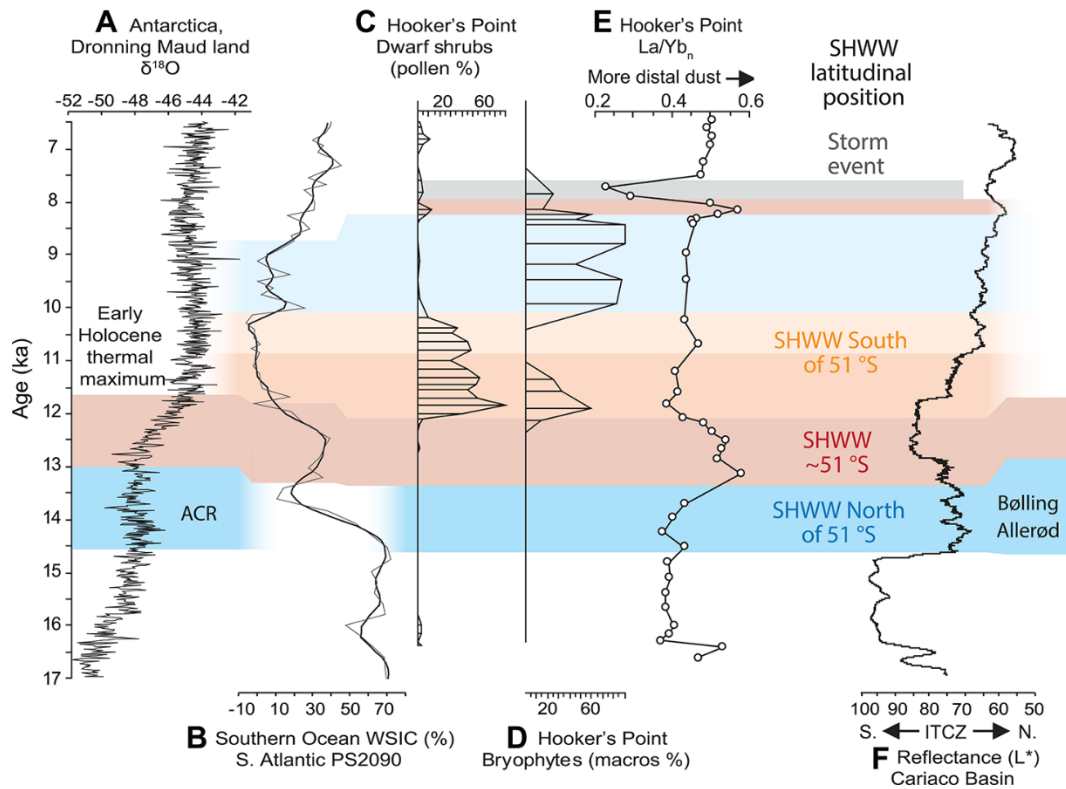


Figure 2. Data from Hooker's Point (Falkland Islands) peat sequence and paleoenvironmental records described in the text. (A) Antarctic ice-core $\delta^{18}\text{O}$ record (Barbante et al., 2006). (B) South Atlantic winter sea-ice concentration (WSIC; Bianchi and Gersonde, 2004). (C) Dwarf shrub pollen abundance. (D) Bryophyte macrofossil abundance. (E) La/Yb_n ratio from Hooker's Point. (F) Cariaco Basin (offshore Venezuela) sediment reflectance record (Deplazes et al., 2013). ACR—Antarctic Cold Reversal; SHWW—Southern Hemisphere westerly wind belt; ITCZ—Intertropical Convergence Zone.

10. 格陵兰冰芯记录中格陵兰变暖时间的综合不确定性估计



翻译人：刘宇星 11811211@mail.sustech.edu.cn

Myrvoll-Nilsen E, Riechers K, et al. Comprehensive uncertainty estimation of the timing of Greenland warmings in the Greenland ice core records [J] Clim. Past, 2022(18), 1275.

<https://doi.org/10.5194/cp-18-1275-2022>

摘要：古气候代理记录具有不可忽略的不确定性，这些不确定性来自代理指标的测量和测年过程。了解测年不确定性对于严格的进一步分析很重要，例如，用于识别和测量格陵兰冰芯记录中冰期-间冰期的转换，用于比较不同代理指标中的可变性，以及用于模型数据一般比较。在这项研究中，我们开发了一个统计框架，使用 2005 年格陵兰冰芯年代学(GICC05)的示例来量化统计层数代理数据中的测年不确定性。我们将每个深度间隔的层计数表示为表示底层物理过程和层计数偏差结构化分量的总和，由回归模型描述，并表示底层物理过程波动的噪声分量，以及无偏计数错误。然后可以对照年表（例如 GICC05）进行采样，通过多元高斯过程来描述所有深度的测年不确定性。我们展示了如何将潜在计算偏差的影响纳入我们的框架。此外，我们提出了对格陵兰冰芯中所证明的 Dansgaard-Oeschger 事件发生时间的精确估计，以及对这些时间的完全不确定性量化。

ABSTRACT: Paleoclimate proxy records have non-negligible uncertainties that arise from both the proxy measurement and the dating processes. Knowledge of the dating uncertainties is important for a rigorous propagation to further analyses, for example, for identification and dating of stadial-interstadial transitions in Greenland ice core records during glacial intervals, for comparing the variability in different proxy archives, and for model-data comparisons in general. In this study we develop a statistical framework to quantify and propagate dating uncertainties in layer counted proxy archives using the example of the Greenland Ice Core Chronology 2005 (GICC05). We express the number of layers per depth interval as the sum of a structured component that represents both underlying physical processes and biases in layer counting, described by a regression model, and a noise component that represents the fluctuations of the underlying physical processes, as well

as unbiased counting errors. The joint dating uncertainties for all depths can then be described by a multivariate Gaussian process from which the chronology (such as the GICC05) can be sampled. We show how the effect of a potential counting bias can be incorporated in our framework. Furthermore we present refined estimates of the occurrence times of Dansgaard–Oeschger events evidenced in Greenland ice cores together with a complete uncertainty quantification of these timings.

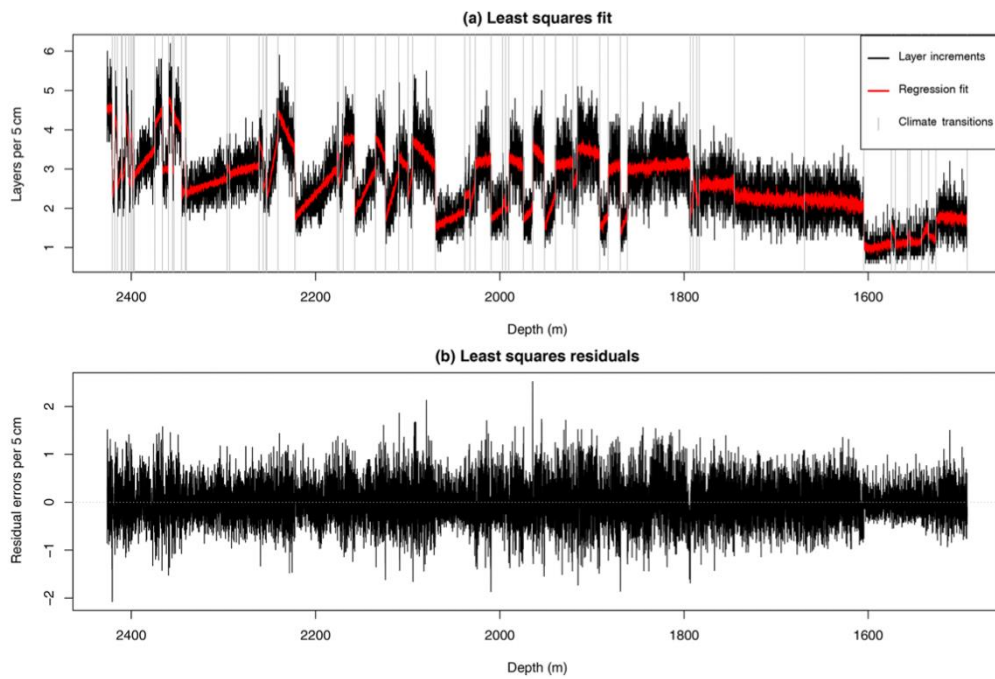


Figure 1. (a) Number of layers counted in the GICC05 time scale per 5 cm depth increments in the NGRIP ice core (black). The red line shows the fitted values from the regression model $a(z_k, x_k) = bz_k^2 + b_x x(k) + \sum_{i=1}^p \psi_i(z_k; a_i, c_i)$. The vertical gray lines represent the transitions between Greenland stadials and interstadials. (b) The residuals δk obtained from fitting the regression model $a(z_k, x_k)$ to the layer increments Δy_k .

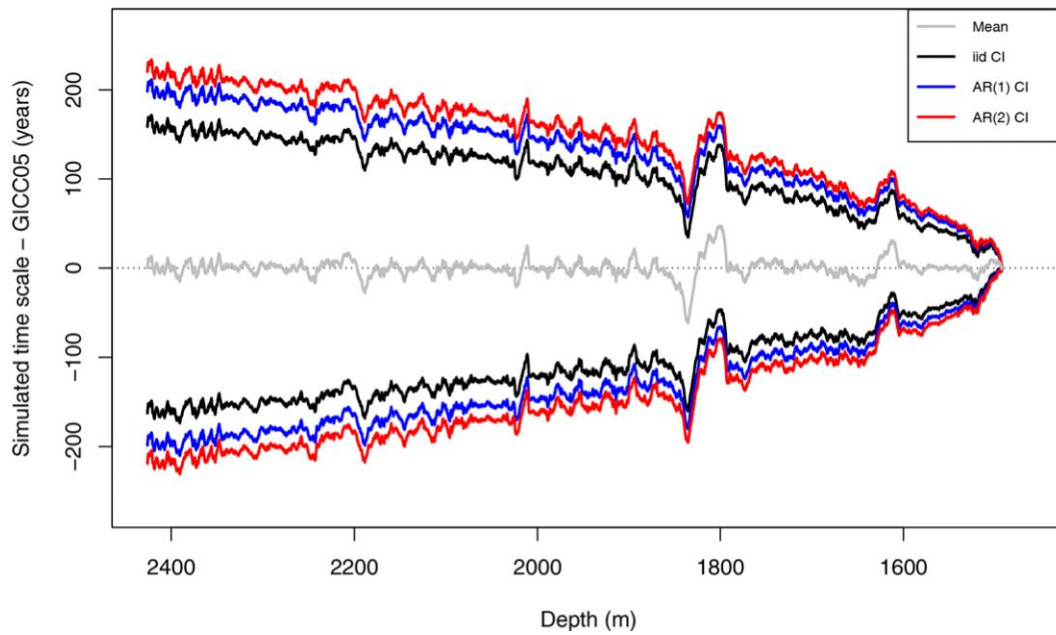


Figure 2. The 95% credible intervals of the dating uncertainty distribution when $\delta^{18}\text{O}$ is used as the proxy covariate. The GICC05 time scale has been subtracted and the noise is modeled using iid (black), AR(1) (blue), and AR(2) (red) noise models. Only the posterior marginal mean computed using AR(1) distributed noise is included (gray) since it is very similar to the mean obtained using other noise assumptions.